NIPES

Journal of Science and Technology Research

Journal homepage: www.nipesjournals.org.ng

Impact of In situ Stress on a Sandstone Reservoir Development In the Niger Delta

Osagie Ehiosu Wilfred [a] **, *Onaiwu David Oduwa*** [b] **, *Oghenovo Omovigho Bright*** [c]

[a,b,c]*Department of Petroleum Engineering,* University *of Benin, Nigeria.*

ARTICLE INFORMATION

Article history:
Received 04 June 2021
Revised 28 June 2021
Accepted 15 September 2021
Available online 20 September 2021

Keywords:
Insitu stress, Geomechanics, Pore pressure, Failure mechanism, Wellbore stability, Niger Delta

ABSTRACT

This project evaluates insitu stresses and her impact on sandstone reservoir development using a field in the Niger Delta and presents a well-scale geo mechanical model to address the pore pressure, geopressures and borehole stability. The rock strength and elastic properties were evaluated using logs and relevant models, an average vertical stress gradient of 0.9PSI/feet is interpreted from the extrapolated density logs. The hydrostatic pressure gradient of 0.43 PSI/feet. Pore pressure against the shales are estimated by Eaton's disequilibrium compaction method, which are found to be mildly overpressure (0.45 psi/feet). The minimum horizontal stress (σ_h) gradient ranges between 0.59 and 0.81 psi/feet. Wellbore stability is shown to be a function of the insitu stress as addressed by the Mogi failure model and the assessed failures are corroborated with the caliper log observations. Safe and effective downhole pressure window is calculated from the interpreted pore pressure, collapse pressure and minimum horizontal stress (σ_h) to avoid any kick, loss or compressive wellbore failures by optimum mud weight designing. Inferences on drilling are discussed which will be helpful for better reservoir development and be a foundation for the mode of EOR processes to be carried out in future.

1. Introduction

This study investigates sandstone reservoir development in the Niger delta and the reservoir development process is the basis for economic and effective development of hydrocarbon reservoirs and enhancing oil recovery. The success or failure of reservoir development largely depends on the research degree of reservoir development geology. These geological and petrophysical properties such as lithology, porosity, permeability and density that can make or mar reservoir development have been found in recent time to be shaped by more fundamental geomechanical properties.

In situ stresses have been widely used to estimate reservoir properties and as such are sacrosanct for reservoir development of which sandstone our reservoir of focus is of no exception. Sandstone reservoirs accumulation and development on the surface are largely determined by the magnitude of her porosity and permeability. The stress orientation is also very important to reservoir permeability.

The geomechanical property to be looked into is the in-situ stress as the key component of a comprehensive geomechanical model is knowledge of the current state of stress [1] In situ stress state is the original stress status in the rock before excavations or other perturbations. In situ stresses are also called far- field stresses. As a first approximation, one can assume that the three principal stresses of a natural in situ stress field are acting vertically (one component, σ_v) and horizontally (two components, σ_h and σ_H) [2].

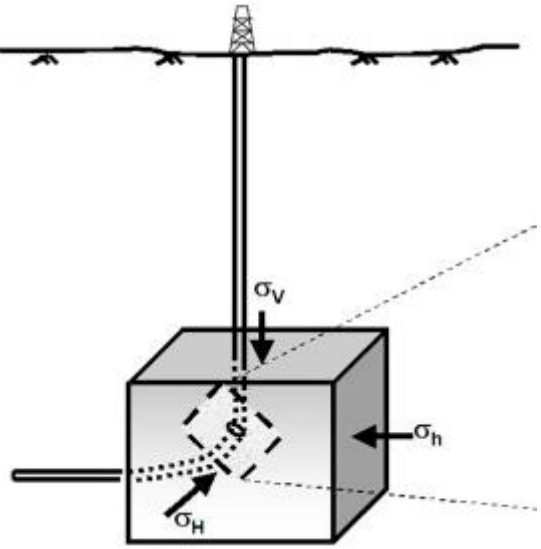

Figure 1 Schematic of the various insitu stresses in the reservoir

The study area, the Niger Delta basin is a normal fault stress regime, constraining the magnitude of the in situ stress is based on the assumption that the three principal stresses at depth are the vertical, maximum horizontal and minimum horizontal stresses even though stress is a tensor with six independent components [3].

In-situ stress data plays a crucial role in various stages of oil and gas well planning, construction, operation and production, in operations which include drilling, well completion, well stimulation, production, and wasted re-injection. Knowledge of in-situ stresses and mechanical properties of the rock formation are vital for the assessment of wellbore construction and production[4]. In situ stresses have been found to have a direct influence on the petrophysical properties of a reservoir [5,6,7].

The need to better understand the behavior of the reservoir has become increasingly essential. It has been recognized that in-situ stress magnitudes have an effect on petrophysical properties of a reservoir but their overall impact on reservoir development isn't clear cut most especially in sandstone reservoir.
Despite their critical importance, the acquisition of in situ stresses has not received much attention and sometimes little attempt is made to collect this significant information [8] of which the Niger delta is no exception. This study therefore gives a holistic outlook that shows not just how in-situ stress shapes reservoir development but how it helps reduce uncertainties in wellbore construction. This study aims to determine the impact of in-situ stresses on sandstone reservoir development in the Niger Delta by determining the in-situ stress using relevant method and models, thorough

analysis on the impact of the in-situ stress on reservoir properties, thorough analysis on the impact on the stability of the wellbore drilled in the reservoir.

2. Methodology

2.1 Techlog software

The techlog schlumberger software was used in this study to aggregate the wellbore information by plotting and interpreting the logs to determine a host of information and trends needed various computations to help achieve the pre-stated objectives.

2.2 Well Logs

The logs used from the dataset of well six in the Niger delta field were comprising majorly of sonic logs (compressional and shear sonic log), density, gamma ray log and the resistivity logs. Although other logs were employed for subsequent calculations such as the porosity log, the shale volume log etc.

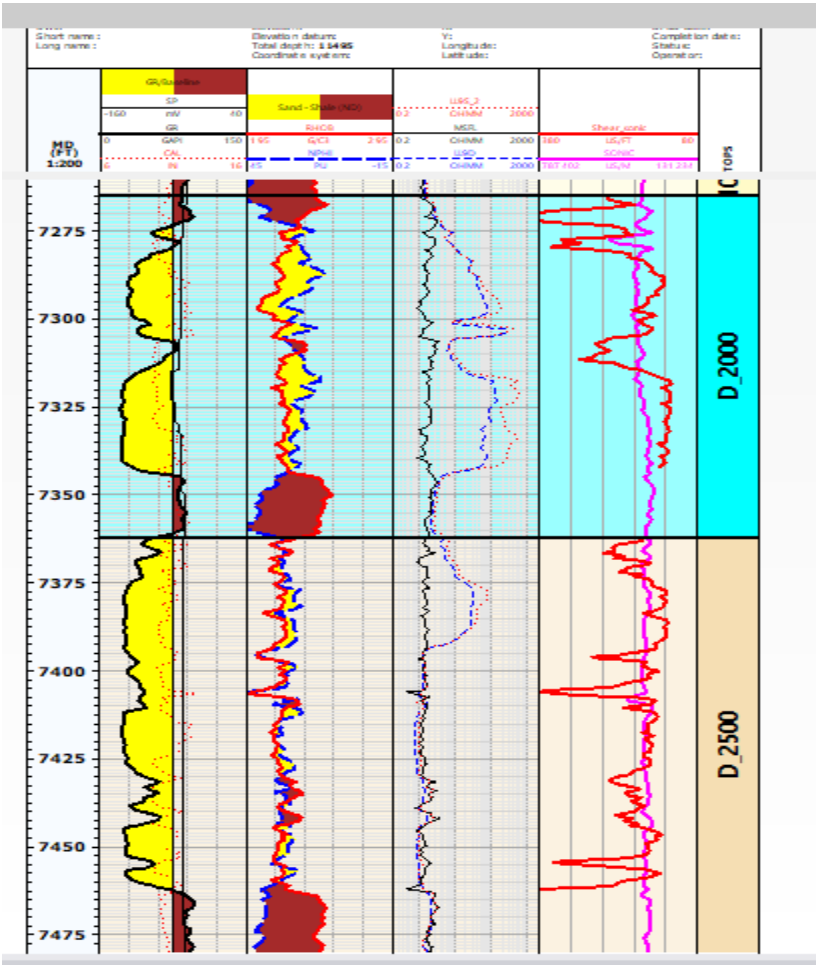

Figure 1 log view of well 06

2.3 Dynamic Elastic Properties

The elastic properties of the Rocks (Young's Modulus (E), shear modulus) (G) and Poisson's ratio (ν)) were calculated using logs (sonic and density log) and standard correlations models.

$$G_{dyn} = 13474.45\frac{\rho b}{(\Delta ts)2} \quad (1)$$

$$K_{dyn} = 13474.45\frac{\rho b}{(\Delta tc)2} - \frac{4}{3}G_{dyn} \quad (2)$$

$$E_{dyn} = \frac{9Gdyn\ Kdyn}{Gdyn + 3Kdyn} \quad (3)$$

$$\nu_{dyn} = \frac{3Kdyn - 2Gdyn}{6Kdyn + 2Gdyn} \quad (4)$$

The dynamic youngs modulus were converted to the workable static youngs modulus using Eissa and Kazi model for Sedimentary rocks.

$$E_s = 0.74E_{dyn} - 0.82 \quad (5)$$

2.4 Rock Strength Parameters

Compute the Rock Strength Parameter (Unconfined compressive strength and Internal friction angle (φ)
UCS was obtained using the static young's modulus correlation under the rock properties section of the Geomechanics module for techlog software.

Internal friction angle φ was obtained using the friction angle from gamma ray log tool under the rock properties section of the Geomechanics module for techlog software.

Energy density is dependent on the diffusivity, particle radius, thickness and specific modulus.

2.5 Vertical stress

The overburden stress or vertical stress is calculated using

$$\sigma_v = \int_0^z \rho(z)gdz \quad (6)$$

Since the density logs (RHOB) typically records only at deeper intervals (is not logged from the surface), a synthetic density log is built and constrained using the indicative trends observed in the available section to compute for the vertical stress using the above formula.
The overburden/vertical stress tool under the geomechanics module has several models to execute this task such as the Extrapolated density, Amoco density, Gardner density, Miller density etc.
The miller density was used having shown to be best fit with our density log.

2.6 Pore pressure

The pore pressure is obtained using the pore pressure wizard tool in the geomechanics section.
The Eaton's relationship is given as:

$$P_{pg} = OBG - (OBG - G_{hyd})\left(\frac{NCT}{DT}\right)^3 \quad (7)$$

Hydrostatic pore pressure gradient was calculated as **0.43psi/ft** from the well plot of hydrostatic pressure against depth

Considering that the NCT can be tricky to determine from log the non-linear depth dependent equations for the normal values in Eaton's method published by Zhang (2011) reformulates the equation to

$$P_{pg}=OBG-(OBG-G_{hyd})\left(\frac{Dm+(Dml-Dm)\exp(-cZ)}{Dt}\right)^3 \quad 8$$

Pore pressure gradient was computed as **0.45 psi/ft**

2.7 Minimum and maximum horizontal stresses

The minimum and maximum horizontal stresses were computed using Mohr-coloumb stress model using the horizontal stress segment of the geomechanics section in techlog. In which the stresses are functions of friction angle vertical stress and pore pressure.

2.8 Failure mechanism

2.8.1 Mogi Coulomb model

The Mogi Coulomb model as reformulated into a linear function by [9] is used ahead of others such as Mohr-Coulomb (which underestimates rock strength), Drucker-Prager (which overestimates rock strength) etc having proven to be most accurate [10].

2.8.1.1 Shear failure

Stress at which Shear failure will occur leading to borehole collapse
These induced principal stresses(tangential(hoop) σ_θ , radial σ_r , axial σ_z) are a function of the insitu stress and for shear failure or breakouts to occur the magnitude of stress are calculated using the equations as presented by [11].

$$\sigma_\theta = 3\sigma_H - \sigma_h - p_w \quad 9$$

$$\sigma_r = p_w \quad 10$$

$$\sigma_z = \sigma_v + 2v(\sigma_H - \sigma_h) \quad 11$$

For failure computation

$$\sigma_m = \frac{\sigma 1+\sigma 3}{2} \quad 12$$

$$c = UCS(1-\sin(\varphi))/(2\cos(\varphi)) \quad 13$$

$$q = (1+\sin(\varphi))/(1-\sin(\varphi)) \quad 14$$

$$\tau oct = a+b\sigma_m \quad 15$$

$$a = \frac{2\sqrt{2}\,c}{3(q+1)} \quad 16$$

$$b = \frac{2\sqrt{2}\,(q-1)}{3(q+1)} \quad 17$$

2.9 Safe mud window for drilling

The safe mud window will be between the mud weight corresponding to pore pressure and that corresponding to the minimum horizontal stress. The safe and stable window lies between mud weight from shear stress and that corresponding to the minimum horizontal stress. (Shear failure is usually caused by low pressure because of a too low mud weight stress at which Shear failure will occur leading to borehole collapse is therefore used as a lower boundary for mud weight design)

as calculated from the Mogi coulomb model and the mud weight corresponding to the point of tensile failure (used as an upper boundary for mud weight design).

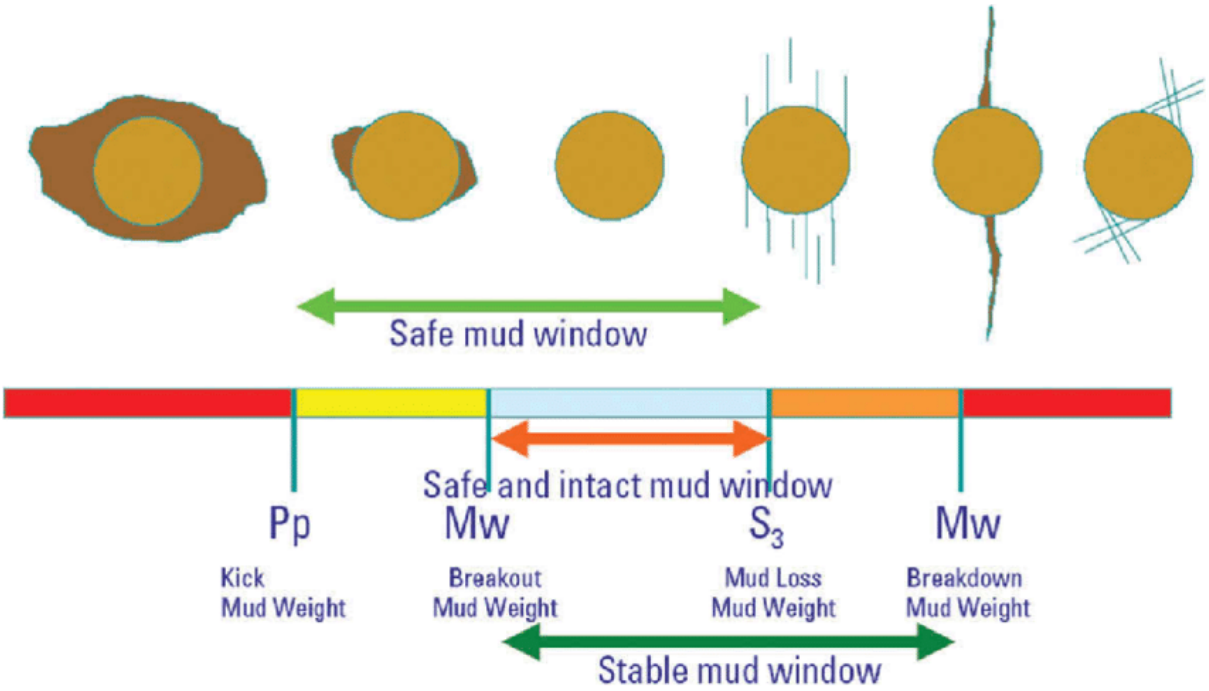

Figure 3 Safe mud window

[12]

3. Results and Discussion

Data editor

Estatic = (0.74*Edyn)-0.82

XWELL 06.Dataset_1

	MD	Edyn	Estatic	Gdyn	Kdyn	PORDEN	RHOB	Shear_sonic	SONIC	Vdyn	Vs	VSH_GR
15304	7652	2.855531	1.178871	1.245607	1.345324	0.2557577	2.228	155.2467	99.933	0.1462401	1.974276	0.05450001
15305	765...	2.771518	1.120062	1.174161	1.444456	0.2648485	2.213	159.3611	99.532	0.180212	1.923304	0.05149999
15306	7653	2.55654	0.9695777	1.029701	1.647672	0.2824243	2.184	169.0543	98.704	0.2413988	1.813027	0.05128572
15307	765...	2.448447	0.8939128	0.9666206	1.74763	0.2909091	2.17	173.9231	98.13	0.2664984	1.762273	0.05
15308	7654	2.407136	0.8649951	0.9523255	1.698659	0.2957577	2.162	174.9003	99.065	0.2638199	1.752427	0.04014285
15309	765...	2.505853	0.9340971	1.0271	1.490877	0.2884849	2.174	168.8803	101.199	0.2198681	1.814895	0.03221427
15310	7655	2.324958	0.8074704	0.9556956	1.366189	0.3006061	2.154	174.2684	104.843	0.2163693	1.758782	0.02257143
15311	765...	2.376084	0.843259	0.970227	1.437433	0.3012121	2.153	172.9183	103.065	0.2244991	1.772514	0.0142143
15312	7656	2.725633	1.087943	1.157778	1.406837	0.2781819	2.191	159.685	100.029	0.1770967	1.919404	0.01335714
15313	765...	2.785311	1.129717	1.219508	1.296632	0.2703031	2.204	156.0519	100.803	0.1419813	1.96409	0.01571429
15314	7657	2.582561	0.987793	1.097914	1.328979	0.2806061	2.187	163.8309	102.72	0.1761221	1.870832	0.02921429
15315	765...	2.377743	0.8444204	0.961198	1.506033	0.2909091	2.17	174.413	102.416	0.2368646	1.757323	0.05235716
15316	7658	2.174929	0.7024505	0.8448454	1.703229	0.2963637	2.161	185.6497	101.441	0.2871758	1.650959	0.08664286
15317	765...	2.232659	0.7428613	0.8676168	1.744227	0.2854547	2.179	183.9586	100.602	0.286662	1.666136	0.1121428
15318	7659	2.297314	0.78812	0.8957028	1.759657	0.2793941	2.189	181.4665	99.926	0.2824088	1.689017	0.1194286
15319	765...	2.368732	0.8381124	0.9389757	1.654176	0.2733335	2.199	177.6401	100.974	0.2613382	1.725399	0.1202857
15320	7660	2.428426	0.8798984	0.9760551	1.58101	0.2684849	2.207	174.5499	101.573	0.2440006	1.755945	0.1202857
15321	766...	2.353867	0.827707	0.9501384	1.501365	0.2721213	2.201	176.6738	103.506	0.2386971	1.734836	0.1194286
15322	7661	2.313651	0.7995556	0.9409002	1.425476	0.2751515	2.196	177.3372	105.076	0.2294879	1.728345	0.1134286
15323	766...	2.413676	0.8695735	0.9765076	1.523046	0.2751515	2.196	174.074	102.343	0.2358718	1.760746	0.09800001
15324	7662	2.595345	0.9967414	1.056796	1.58988	0.2696971	2.205	167.6734	99.535	0.2279307	1.827958	0.08235713
15325	766...	2.684018	1.058813	1.095345	1.627819	0.2690909	2.206	164.7338	98.107	0.2251928	1.860577	0.06864286
15326	7663	2.568943	0.9782601	1.034819	1.654728	0.2824243	2.184	168.6357	98.478	0.2412523	1.817527	0.04914286
15327	766...	2.428288	0.8798015	0.9519772	1.801869	0.3000001	2.155	174.6489	97.236	0.2753918	1.754949	0.02621427

Figure 4 Elastic properties computation for well 6

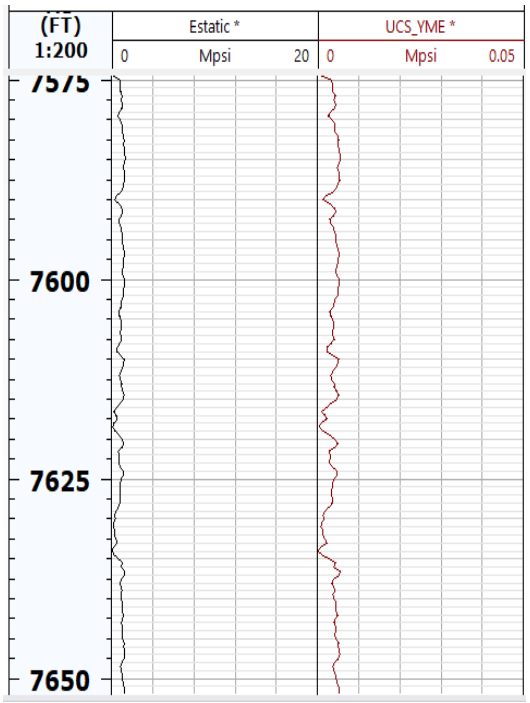

Figure 5 Log view of UCS

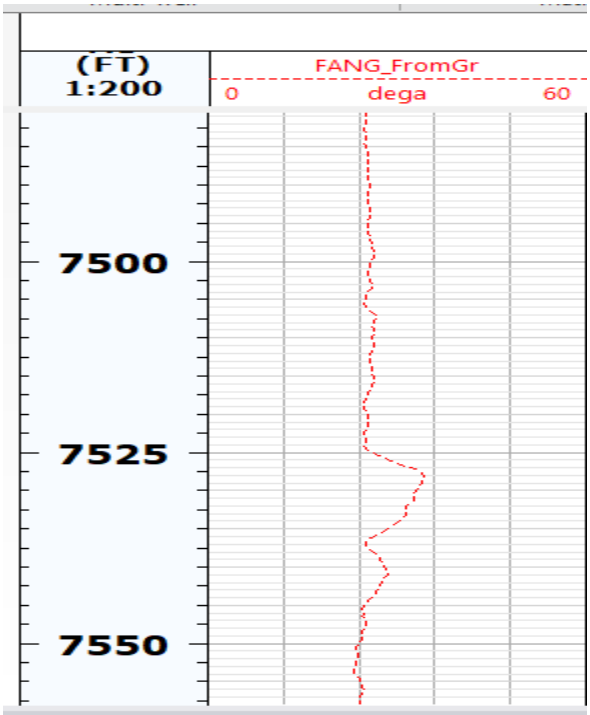

Figure 6 Log view of friction angle

from static young modulus from gamma ray log

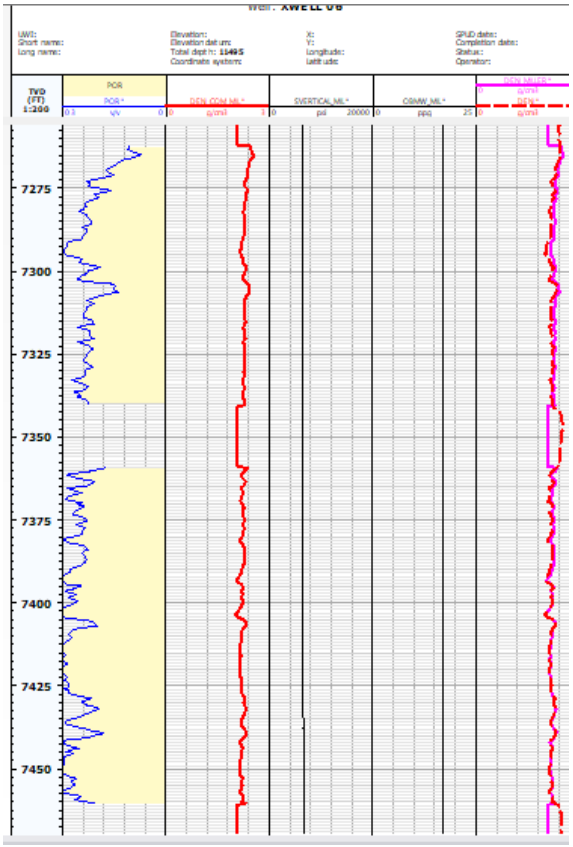

Figure 7 synthetic density and overburden stress for well 6 from Miller correlation

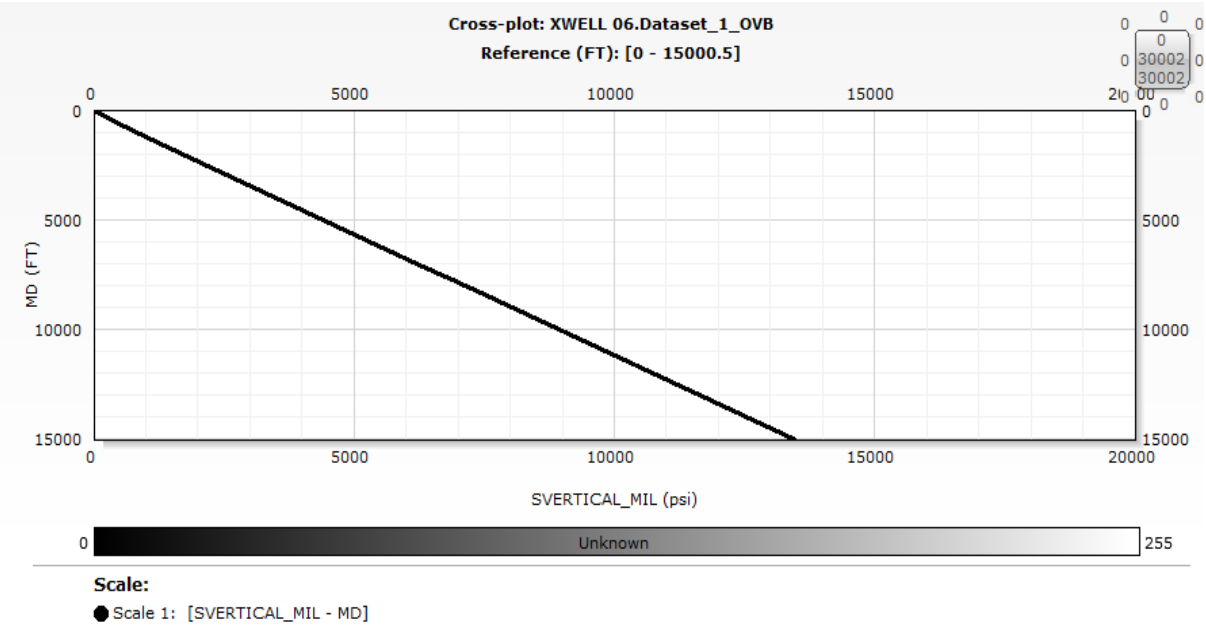

Figure 8 Vertical/overburden stress plot

The overburden/vertical stress gradient was calculated as **0.9 psi/ft**

The pore pressure gradient was calculated to be **0.45psi/ft**

The vertical stress was used to estimate the pore pressure and pore pressure gradient to aid our understanding of the geo pressure regime (over pressure) our pore pressure gradient was calculated as 0.45ppg indicating a mild overpressure therefore the shale sections of the well will be prone to hydrofractures and sand injectites structures(formation of structures by sediment injection)

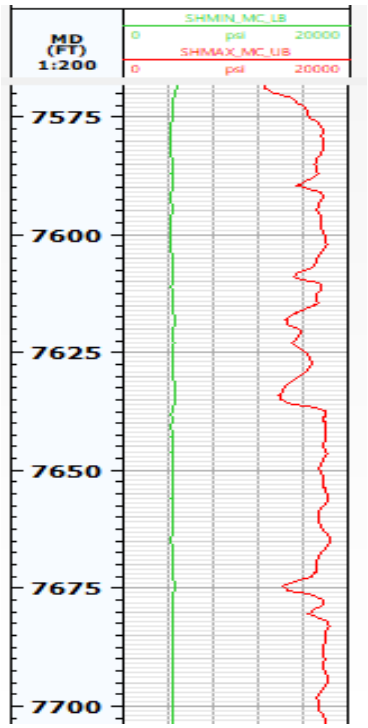

Figure 9 Log view of minimum and maximum horizontal stress

The minimum horizontal stress was found to have a gradient in the range of **0.59-0.81psi/ft**

Data editor

cohesion = (UCS_YME*(1-sin(FANG_FromGr/57.296)))/(2*cos(FANG_FromGr/57.296))

XWELL 06.Dataset_1

	MD	axial_stress	cohesion	FANG_FromGr	hoop_stress	PPRS_NORM	radial_stress	SHMAX_MC_UB	SHMIN_MC_LB	stress_median	SVERTICAL_MIL	UCS_YME	Vdyn
15485	7742.5	12380.12	1085.939	38.6075	49279.39	3482.938	3482.938	19026.19	4316.23	26381.17	7081.835	4513.569	0.1800918
15486	7743	11268.95	1226.289	38.47531	49003.56	3483.163	3483.163	18936.05	4321.443	26243.36	7082.309	5081.905	0.1432347
15487	7743.5	12007.35	1137.724	38.28688	48612.52	3483.388	3483.388	18808.23	4328.791	26047.95	7082.786	4695.14	0.1700537
15488	7744	12170.16	1067.435	38.10969	48248.75	3483.613	3483.613	18689.37	4335.755	25866.18	7083.26	4387.771	0.1771993
15489	7744.5	14090.14	903.0781	37.97469	47974.77	3483.838	3483.838	18599.92	4341.153	25729.3	7083.732	3701.082	0.2456875
15490	7745	13855.39	943.3295	37.76656	47554.57	3484.062	3484.062	18462.67	4349.361	25519.32	7084.196	3848.295	0.239887
15491	7745.5	12250.8	1108.678	37.50781	47038.18	3484.288	3484.288	18294.01	4359.571	25261.24	7084.663	4497.111	0.1853729
15492	7746	12568.44	1055.365	37.38125	46790	3484.512	3484.512	18213.08	4364.741	25137.26	7085.139	4268.966	0.1979767
15493	7746.5	12702.46	996.9688	37.4825	46994.24	3484.738	3484.738	18280.03	4361.118	25239.49	7085.612	4041.736	0.2017702
15494	7747	11057.21	1132.738	37.56969	47171.47	3484.962	3484.962	18338.16	4358.045	25328.22	7086.084	4600.967	0.1420278
15495	7747.5	8400.312	1256.863	37.58937	47214.16	3485.188	3485.188	18352.31	4357.575	25349.68	7086.561	5107.354	0.04693735
15496	7748	10336.3	1262.717	37.14781	46343.72	3485.413	3485.413	18068.03	4374.949	24914.57	7087.045	5081.626	0.1186459
15497	7748.5	12993.08	1115.822	36.41656	44945.83	3485.637	3485.637	17611.84	4404.046	24215.73	7087.529	4419.479	0.223563
15498	7749	12768.15	1192.194	35.80625	43821.45	3485.863	3485.863	17245.4	4428.879	23653.66	7088.011	4660.117	0.2215946
15499	7749.5	13347.11	1141.245	35.25219	42832.44	3486.087	3486.087	16923.46	4451.854	23159.26	7088.5	4408.271	0.2509142
15500	7750	15082.79	705.9756	34.42812	41412.62	3486.312	3486.312	16461.84	4486.602	22449.46	7088.99	2679.59	0.3337636
15501	7750.5	15662.9	417.3793	33.57312	40002.34	3486.538	3486.538	16004.15	4523.568	21744.44	7089.474	1555.938	0.3733883
15502	7751	15096.28	529.5059	32.85594	38866.52	3486.762	3486.762	15636.22	4555.37	21176.64	7089.956	1944.618	0.3612687
15503	7751.5	13302.76	1049.793	32.39188	38154.22	3486.988	3486.988	15405.88	4576.427	20820.6	7090.446	3818.483	0.2868249
15504	7752	13013	1139.214	32.15562	37799.41	3487.212	3487.212	15291.35	4587.417	20643.31	7090.955	4123.578	0.2766293
15505	7752.5	13044.24	1223.529	32.24281	37933.94	3487.438	3487.438	15335.05	4583.78	20710.69	7091.469	4436.742	0.2768402
15506	7753	12408.28	1349.37	32.6	38481.93	3487.663	3487.663	15512.54	4568.017	20984.79	7091.983	4929.337	0.242875
15507	7753.5	10105.46	1525.416	33.54219	39970.66	3487.887	3487.887	15995.1	4526.746	21729.28	7092.499	5682.876	0.1313599
15508	7754	7852.657	1508.486	34.31	41238.74	3488.113	3488.113	16406.96	4494.032	22363.43	7093.015	5711.304	0.03188307

Figure 10 Computation for induced principal stress

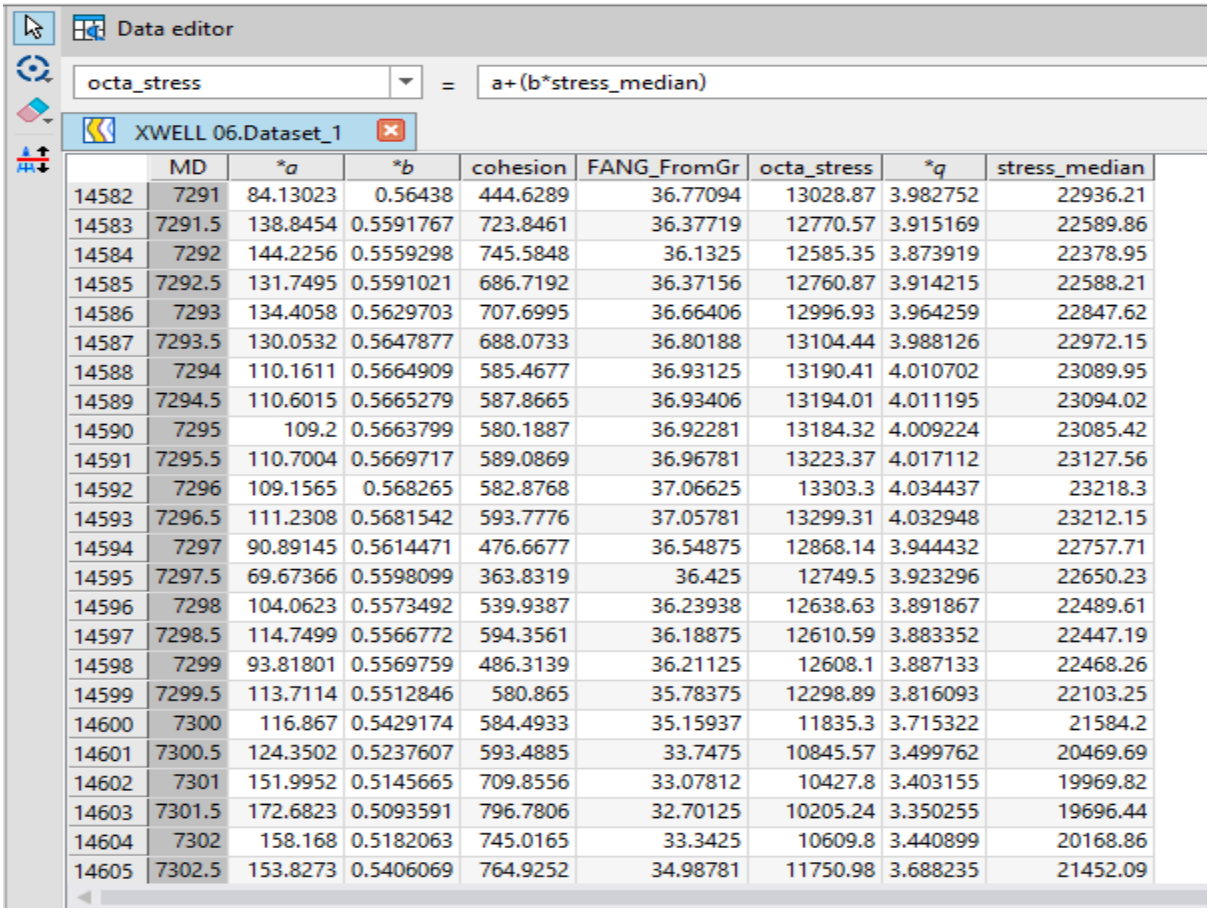

	MD	*a	*b	cohesion	FANG_FromGr	octa_stress	*q	stress_median
14582	7291	84.13023	0.56438	444.6289	36.77094	13028.87	3.982752	22936.21
14583	7291.5	138.8454	0.5591767	723.8461	36.37719	12770.57	3.915169	22589.86
14584	7292	144.2256	0.5559298	745.5848	36.1325	12585.35	3.873919	22378.95
14585	7292.5	131.7495	0.5591021	686.7192	36.37156	12760.87	3.914215	22588.21
14586	7293	134.4058	0.5629703	707.6995	36.66406	12996.93	3.964259	22847.62
14587	7293.5	130.0532	0.5647877	688.0733	36.80188	13104.44	3.988126	22972.15
14588	7294	110.1611	0.5664909	585.4677	36.93125	13190.41	4.010702	23089.95
14589	7294.5	110.6015	0.5665279	587.8665	36.93406	13194.01	4.011195	23094.02
14590	7295	109.2	0.5663799	580.1887	36.92281	13184.32	4.009224	23085.42
14591	7295.5	110.7004	0.5669717	589.0869	36.96781	13223.37	4.017112	23127.56
14592	7296	109.1565	0.568265	582.8768	37.06625	13303.3	4.034437	23218.3
14593	7296.5	111.2308	0.5681542	593.7776	37.05781	13299.31	4.032948	23212.15
14594	7297	90.89145	0.5614471	476.6677	36.54875	12868.14	3.944432	22757.71
14595	7297.5	69.67366	0.5598099	363.8319	36.425	12749.5	3.923296	22650.23
14596	7298	104.0623	0.5573492	539.9387	36.23938	12638.63	3.891867	22489.61
14597	7298.5	114.7499	0.5566772	594.3561	36.18875	12610.59	3.883352	22447.19
14598	7299	93.81801	0.5569759	486.3139	36.21125	12608.1	3.887133	22468.26
14599	7299.5	113.7114	0.5512846	580.865	35.78375	12298.89	3.816093	22103.25
14600	7300	116.867	0.5429174	584.4933	35.15937	11835.3	3.715322	21584.2
14601	7300.5	124.3502	0.5237607	593.4885	33.7475	10845.57	3.499762	20469.69
14602	7301	151.9952	0.5145665	709.8556	33.07812	10427.8	3.403155	19969.82
14603	7301.5	172.6823	0.5093591	796.7806	32.70125	10205.24	3.350255	19696.44
14604	7302	158.168	0.5182063	745.0165	33.3425	10609.8	3.440899	20168.86
14605	7302.5	153.8273	0.5406069	764.9252	34.98781	11750.98	3.688235	21452.09

Figure 11 Computation for octahedral stress

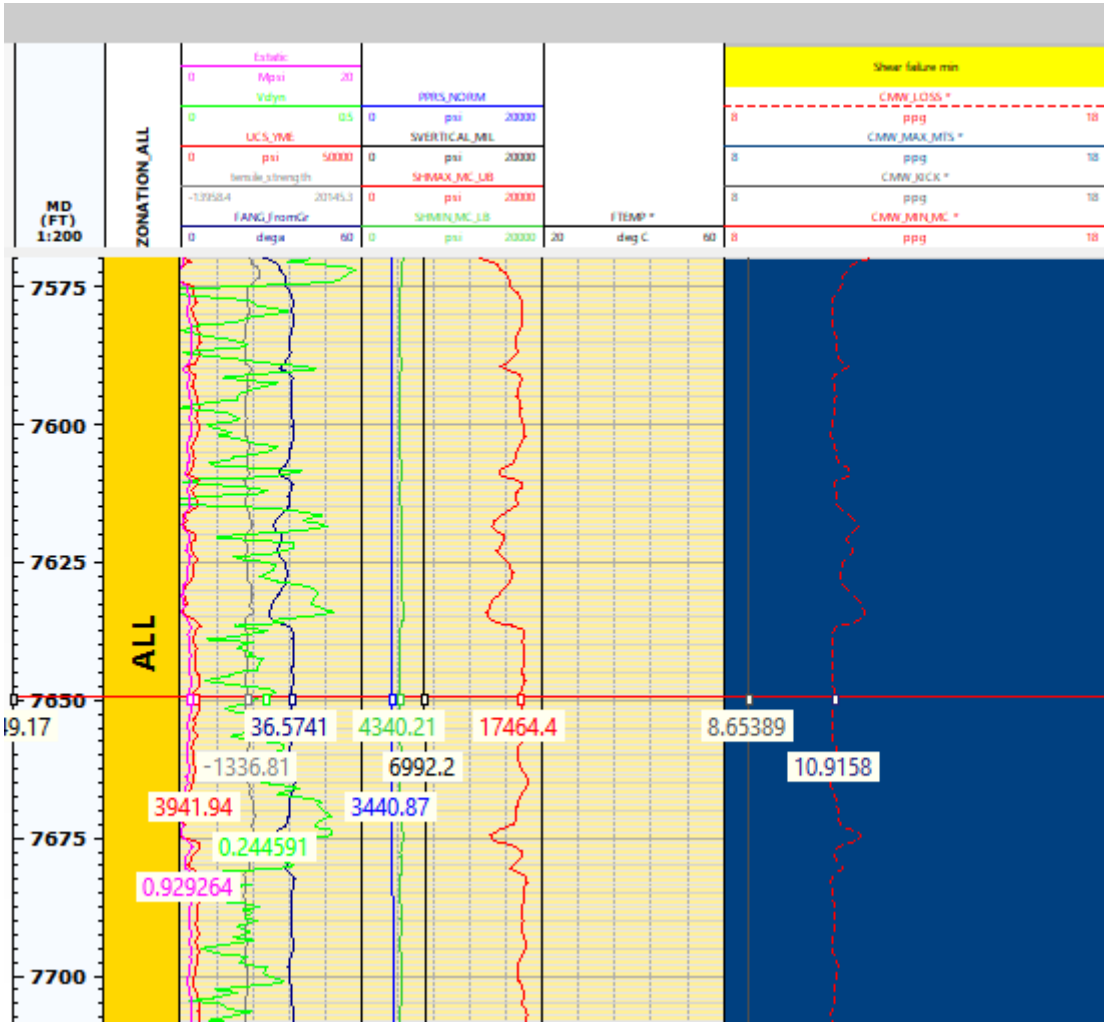

Figure 12 Equivalent mud weight from minimum horizontal stress

The various mud weights were computed to obtain the following
Kick mud weight from pore pressure averaged 8.7ppg
Mud weight from shear stress averaged 9.5 ppg
Mud weight from minimum horizontal stress ranged from 9.75ppg to 11ppg upper sections of the well and 11-12.78 in the lower well sections inclusive of our reservoir
Mud weight from Tensile strength averaged 14.7ppg

Table 1 Effect of Insitu stress on wellbore stability

Well Section	**Equivalent mud weight (ppg)**	**Implication**
Upper section	<8.7	The well will experience a kick therefore unsafe and unstable
	8.7-9.5	Safe and unstable for drilling i.e the well will be at high risk of breakout especially in the shale section
	9.5-11	Safe and stable for drilling
	11-14.7	Stable but unsafe for drilling due to the challenges that will arise from the well losing fluid to the formation.
	>14.7	Formation breakdown will occur
Lower section	<9	The well will experience a kick therefore unsafe and unstable
	9-10	Safe and unstable for drilling; the well will be at high risk of breakout especially
	10-12.78	Safe and stable for drilling
	12-14.7	Stable but unsafe for drilling due to the challenges that will arise from the well losing fluid to the formation
	>14.7	Formation breakdown will occur

The exercise starts with the determination of elastic properties using (Eqn. 1-5) as shown in (Figure 4) and rock strength properties using logs i.e. UCS (Figure 5) and friction angle (Figure 6) continues with the generation of an overburden/vertical stress (σ_v) profile using the bulk density log (Eqn.6). The bulk-density log was only available from the 4490ft of measured depth interval. So for the top 4490ft, a pseudo density profile was modelled using miller empirical equation found to best model the already logged section, as presented in Figure 7, Average overburden pressure gradient is found to be 0.9PSI/feet, by plotting the calculated σ_v against the burial depth (Figure 8).

The reservoir sandstones are found to have a hydrostatic regime with 0.43 PSI/feet gradient (Figure 6). Pore pressure against the shales are estimated by indirect method (Eaton's equation) having a gradient of 0.45 PSI/feet shale pore pressure gradient. Shales are found to be mildly overpressured.

Horizontal stress σ_h, σ_H is calculated using the Mohr coulomb model (Figure 9), usually, σ_h provides a higher value against the pore pressure intervals. Minimum horizontal stress gradient ranges from 0.5 9–0.81 PSI/feet. It is to be noted that the estimated minimum horizontal stress could not be calibrated due to the unavailability of leak-off test (LOT) or mini-frac tests.

The induced principal stress ((tangential(hoop) σ_θ , radial σ_r , axial σ_z)) were obtained (Eqn. 9-11) on account of the insitu stress computations as shown in Fig.10. and used to compute the

failure mechanism using the Mogi coulomb model which has been found to best estimate shear stress and tensile strength (Eqn. 11-17) as shown in Fig. 11.
A comprehensive wellbore stability analysis was done by converting the pressures (pore pressure, shear stress minimum horizontal stress and tensile strength) into mud weight and understood with information from Fig. 3 as shown in Fig. 12 The various mud weights were computed to obtain the following Kick mud weight from pore pressure averaged 8.7ppg ,Mud weight from shear stress averaged 9.5ppg , mud weight from minimum horizontal stress ranged from 9.75ppg to 11ppg upper sections of the well and 11-12.78 in the lower well sections inclusive of our reservoir, mud weight from Tensile strength averaged 14.7ppg.
To address the wellbore instabilities against the mildly overpressured shales, drilling mud weights need to be kept above the interpreted mud weight from shear stress. We have worked out the sub-surface kick-loss-failure and breakdown windows in Table 1. based on the interpreted pressure gradients. Drilling mud properties for subsequent wells in the area should be designed taking into account the effect of various pressure cum mud weight windows as presented in Table 1.

4. Conclusion

In this paper we have presented a comprehensive insitu stress interpretation from the studied field, Niger Delta. Shales were found to be mildly overpressured with an average pore pressure gradient of 0.45 PSI/ft, a function of the insitu stress (vertical stress). A lithology dependent horizontal stress was estimated from Mohr coulomb model the stresses were used in determining the induced principal stress and by extension the failure criteria at tensile and shear using the Mogi coulomb model.
Her impact was shown on overall wellbore stability with the minimum horizontal stress of gradient 0.59-0.81 psi/ft forming the upper limit for wellbore stability. Depending on the interpreted downhole pressure gradients, an optimum mud weight range was presented to avoid influx and wellbore instabilities. The results of this work will be useful for optimum drilling fluid design for subsequent wells to be drilled in the area.

Nomenclature

A	Coefficient
B	Coefficient
C	Coefficient
C	Formation cohesion Diffusivity
Dm	Reference sonic slowness (μs/ft)
Dml	Mudline sonic slowness (μs/ft)
E_{dyn}	Dynamic youngs modulus (Mpsi)
E_s	Static youngs modulus (Mpsi)
G_{dyn}	Dynamic Shear modulus (Mpsi)
G_{hyd}	Hydrostatic pressure gradient
K_{dyn}	Dynamic bulk modulus (Mpsi)
NCT	Normal compaction trend
OBG	Overburden pressure gradient (psi/ft)
P_p	Pore pressure (psi)
P_{pg}	Pore pressure gradient (Mpsi/ft)
UCS	Unconfined compressive strength(Mpsi)
Vdyn	Poisson ratio
Z	Depth (ft)

Greek letters

Δtc	compressional-wave slowness, μsec/ft
Δts	shear-wave slowness, μsec/ft

σ_h	Minimum horizontal stress (psi)
σ_H	Maximum horizontal stress (psi)
σ_v	Vertical stress (psi)
σ_r	Radial stress (psi)
σ_z	Axial stress (psi)
σ_θ	Hoop stress (psi)
σ_m	Median stress (psi)
σ_1	largest principal stresses (psi)
σ_3	least principal stresses (psi)
ρb	Bulk density g/cm³
φ	Friction angle
τ_0	Tensile strength (psi)
Toct	Octahedral shear stress (psi)

References

[1] Zoback, M.D. 2007. Reservoir geomechanics: earth stress and rock mechanics applied to exploration, production and wellbore stability. Cambridge: Cambridge Press; 449p.
[2] Zhang, J.J., 2019. Applied petroleum geomechanics. Gulf professional publishing. P.7. https://doi.org/10.1016/B978-0-12-814814-3.00001-0
[3] Abija, A., Ankwo, F. , Tse, T., 2016. In Situ stress magnitude and orientation in an onshore field, Eastern Niger Delta: implications for directional drilling. SPE Nigeria Annual International Conference and Exhibition Lagos, Nigeria. https://doi.org/10.2118/ 184234-MS. Aug 2-4. SPE-184234-MS.
[4] Bernt, S.A, Reza, L., 2011. Petroleum rock mechanics: drilling operations and well design. Gulf professional publishing. P.107. https://doi. org/10.1016/B978-0-12-385546-6.00008-5
[5] Pan, Z., connel, LD., camileri, M, 2010 laboratory characterization of coal reservoir permeability for primary and enhanced coalbed methane recovery. Int. J. coal Geol 82, 252-261
[6] Connnel, L.D., Meng,L Pan, Z., 2010.An analytical coal permeability model for triaxial strain and stress conditions. Int. J. coal Geol 84, 103-114
[7] Zhang, Y., Xu, Lebedev, M., Samrmadivaleh, M., Barifcani, A., Iglauer, S., 2016. Multi scale x-ray computed tomography analysis of coal microstructure and permeability changes as a function of effective stress. Int. J. coal Geol. 165, 149-156.
[8] Bernt, S.A, Reza, L., 2019. Petroleum rock mechanics: drilling operations and well design (second edition). Gulf professional publishing. P. 105. https://doi.org/10.1016/B978-0-12-815903-3.00008-X
[9] Al-Ajmi AM, Zimmerman RW. Relationship between the Mogi and the Coulomb failure criteria. International Journal of Rock Mechanics and Mining Sciences 2005;42(3):431–9.
[10] Al-Ajmi, Adel M. (2012): Mechanical Stability of Horizontal Wellbore Implementing Mogi-Coulomb Law. In Advances in Petroleum Exploration and Development 4 (2), pp. 28–36.
[11] Gholami, R., Moradzadeh, A., Rasouli, V., Hanachi, J., 2014. Practical application of failure criteria in determining safe mud weight windows in drilling operations. Journal of Rock Mechanics and Geotechnical Engineering 6 (1), 13–25. https://doi. org/10.1016/j.jrmge.2013.11.002.
[12] Abdideh, M., Fathabadi, M.R., 2013. Analysis of stress field and determination of safe mud window in borehole drilling(case study: SW Iran). J Petrol Explor Prod Technol doi 10.1007/s13202-013-0053-2.